Jurnal Polimesin
Department of Mechanical Engineering
State Polytechnic of Lhokseumawe
http://e-jurnal.pnl.ac.id/polimesin
e-ISSN : 2549-1999 No. : 3 Month : June
p-ISSN : 1693-5462 Volume : 24 Year : 2026

Processing dates: received on 2025-12-16, reviewed on 2026-3-04, accepted on 2026-04-14 and online availability on 2026-06-30

Development and validation of a modified TM25 journal bearing test equipment for load-carrying capacity and frictional torque measurement

Nurcahya Nugraha*, Jamiatul Akmal, Martinus, Ahmad Su'udi, Rizal Nazarrudin, Eko Wahyu Saputra, Wahyu Adani, Fauzan Azima
Department of Mechanical Engineering, University of Lampung, Bandar Lampung 35145, Indonesia
*Corresponding author: nurcahya.1995@eng.unila.ac.id

Abstract

This study developed and validated a low-cost measurement platform by upgrading an existing TM25 journal bearing demonstration unit. The original apparatus was limited to pressure distribution observation through manometer tubes, whereas the modified system integrated load cells and an Arduino-based data acquisition system to measure load-carrying capacity and frictional torque in real time. Load cell calibration was conducted using an eight-point dead-weight method with three repetitions, resulting in a calibration deviation of less than 2% across the test range. Experimental testing was performed at five rotational speeds (1000–2000 rpm) using three lubricant grades (SAE 10W-30, SAE 10W-40, and SAE 20W-50) to evaluate their influence on bearing performance. The results show that both load-carrying capacity and frictional torque increase with rotational speed and lubricant viscosity, with the highest values obtained using SAE 20W-50. The measured trends agree well with the original TM25 pressure distribution data and are consistent with hydrodynamic lubrication theory. The modified test equipment provides stable and repeatable measurements and extends the functionality of the TM25 unit as an experimental platform for tribology education and journal bearing performance analysis.

Keywords:
Journal bearing, test rig, load-carrying capacity, frictional torque, data acquisition.

1 Introduction

Journal bearings are critical machine elements that support rotating shafts and form a hydrodynamic lubrication film to minimize contact between shaft and bearing. Journal bearings are commonly used in a variety of machine applications, from the automotive, electrical, and manufacturing industries. Two parameters that significantly determine the performance and reliability of journal bearings are frictional torque, and load-carrying capacity, which are related to the ability to support and stabilize the fluid film [1], [2], [3].

In the domain of experimentation and learning, various journal bearing test rigs in educational laboratories, such as the TM25 journal bearing demonstration still focus on visualization of pressure distribution or separate manual measurements, as shown in Fig. 1. TM25 journal bearing demonstration specifications can be seen in Table 1 [4]. This specification makes the real-time acquisition of frictional torque and load-carrying capacity less than optimal. To cover this weakness, it is necessary to upgrade the educational platform using accessible, data-driven technologies. The development and affordability of load cells and open-source microcontrollers (Arduino) now enable these improvements, providing direct monitoring capabilities, relatively low cost, and flexibility to build a real-time and accurate journal bearing performance database [5].

In principle, the measurement of frictional torque on a journal bearing can be realized by measuring the force on the moment arm using a calibrated load cell. Meanwhile, the load-carrying capacity can be monitored through changes in the vertical force measured by a load cell aligned with the eccentricity direction of the journal bearing. The reliability of the test results is greatly influenced by the mechanical design (sensor placement and structural stiffness), calibration procedures, lubricant temperature control, and data acquisition and processing strategies [6], [7], [8].

Recent studies on journal bearings have extensively explored the dynamics of frictional torque and load-carrying capacity through both experimental and numerical approaches [9], [10]. Computational methods, particularly the Finite Element Method (FEM) [11] and finite volume method [12], [13], are frequently used to predict pressure distribution and load-carrying capacity of journal bearing performance. Predictive estimation of the load-carrying capacity and tribological durability of journal bearings has been carried out using numerical and experimental approaches which highlight the importance of validating measurement data in complex bearing systems [18], [19]. To validate these numerical models, reliable and continuous experimental data is highly required. Consequently, on the experimental front, researchers have begun developing advanced condition monitoring systems [14]. Furthermore, from the literature highlights, it is important to monitor frictional torque and load-carrying capacity of journal bearings [15], [16]. From the instrumentation perspective, a microcontroller-based dynamic torque transducer capable of recording torque changes in real-time has been designed and analyzed [17]. This approach can be adapted for developing journal-bearing performance testing tools. Concurrently, providing effective educational tools for bearing analysis is essential [18]. Most existing educational platforms still rely on static or manual measurements, thus limiting the ability to continuously observe transient hydrodynamic behavior and validate theoretical models.

Based on this background, this study aims to develop and modify the TM25 journal bearing demonstration test rig by integrating load cells and Arduino to monitor frictional torque and load-carrying capacity in real-time.

Table 1. TM25 journal bearing demonstration specifications [19]

Part	Details
Operating environment	Indoor (laboratory) Altitude up to 2000 m Temperature range 5°C to 40°C Maximum relative humidity 80% for temperatures up to 31°C, decreasing linearly to 50% relative humidity at 40°C Overvoltage category 2 (as specified in EN61010-1) Pollution degree 2 (as specified in EN61010-1)
Dimensions and weight	2850 mm high × 990 mm wide × 970 mm front to back and 68 kg
Electrical supply	230 VAC 50 Hz or 120 VAC 60 Hz
Oil type	Multigrade 15W/50 or equivalent
Diameter of journal	50 mm
Diameter of bearing	55 mm
Effective width of bearing	70 mm
Overall bearing width	80 mm
Dry weight of bearing	650 g
Volume of oil in bearing	65.5 cm^3
Nominal bearing speed	500 to 3000 rpm

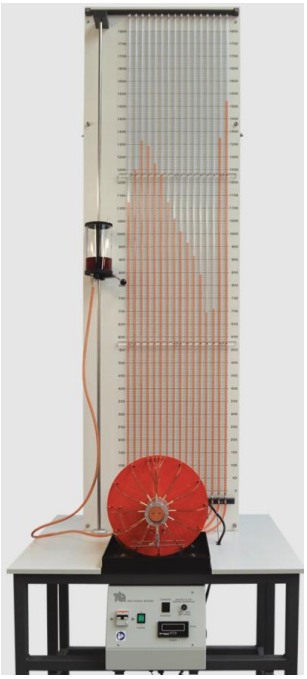

Fig. 1. TM25 journal bearing demonstration [4].

This innovation is expected to improve the quality of experimental data, efficiency of testing time, and contribute to the development of more modern and applicable journal bearing performance test rig in education. The development of this tool can also contribute to a better understanding of the relationship between rotational speed, oil viscosity to the pressure distribution, load-carrying capacity and frictional torque in journal bearings, which are important parameters in lubrication performance.

2 Research method

The research phase begins with identifying requirements, developing design concept, embodiment design, fabrication, and testing. The research flowchart as shown in Fig. 2.

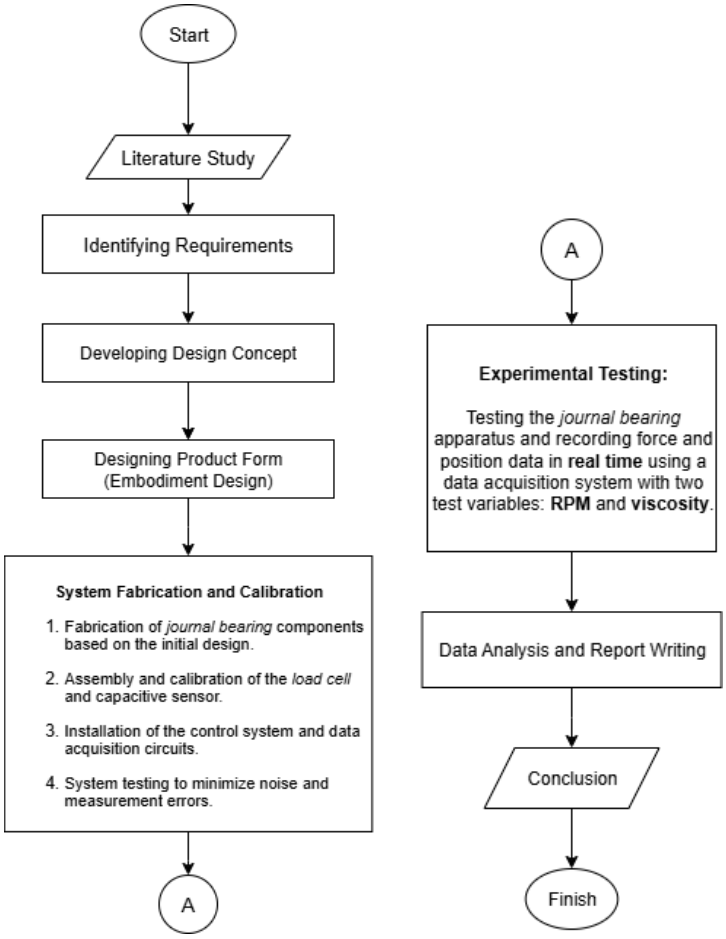

Fig. 2. Research flowchart.

2.1 Needs identification

The initial stage of test equipment development began with the journal bearing's functionality as a support for a rotating shaft with a hydrodynamic damping mechanism. To obtain journal bearing performance, a test device capable of replicating real-world operating conditions and performing real-time, continuous, and calibrated measurements was required. The TM25 journal bearing demonstration demonstrated limitations in measuring load-carrying capacity and frictional torque, as well as in instrumentation: the measurement lacked digital data acquisition. To overcome these limitations, specific quantitative design targets were established for the modified platform. The key design requirements were: (1) a measurable frictional torque range of 0 to 5 Nm; (2) a load-carrying capacity range of 0-10 N; (3) a data acquisition frequency of 10-80 Hz; and (4) a measurement uncertainty of <2%.

The frictional torque was determined by measuring the tangential resistance force generated by the shaft rotating against its bearing, while load-carrying capacity was measured by the vertical force experienced by the bearing during the test. Before modifying the TM25 journal bearing demonstration, several explicit design requirements were established to ensure the reliability of the real-time measurement platform. The design specifications of the measuring instrument are shown in Table 2.

Table 2. Design specifications for measuring load-carrying capacity and frictional torque of journal bearings

Needs aspect	Frictional torque measurement	Load-carrying capacity measurement
Functionality	Measuring the frictional torque between the shaft and bearing	Measuring the load-carrying capacity generated by the lubricant
Measured parameter	Torque (Nm)	Newton (N)
Target load range	0 – 5 N·m	0 – 10 N
Measurement resolution	<0.001 Nm	<0.001 N
Sampling rate	10-80 Hz	10-80 Hz
Installation	Load cell connected to the torque arm	Load cell placed under the bearing housing
Assembly	Can be mounted and removable without major modification at TM25 journal bearing demonstration structure	Can be mounted and removable without major modification at TM25 journal bearing demonstration structure
Room temperature	20–35°C	20–35°C
Rotational speed	0–3000 rpm	0–3000 rpm
Radial alignment	<0.05 mm	<0.05 mm
Additional requirements	Load cell mounting part, load cell calibration, signal amplification	Load cell mounting part, load cell calibration, signal amplification

2.2 Conceptual design

Based on the specifications in Table 2, a design concept was developed as shown in Fig. 3. The development concept for the TM25 journal bearing demonstration focuses on two separate types of measuring instruments, namely for measuring load-carrying capacity and frictional torque. In Fig. 3, the shaft (3) rotates inside the bearing (1) separated by a lubricating fluid (2) to create hydrodynamic pressure. The hydrodynamic force on the bearing is transmitted through the vertical tension bar and the joint to the load cell mounted on a rigid support (15) and locked by a lock nut (14). This configuration produces a vertical force measurement that represents the load-carrying capacity. The actual load-carrying capacity (W) of the journal bearing is determined by the pressure generated within the lubricant film. It is assumed derived only from the vertical force (F_v) reading of the load cell. Based on the static equilibrium of the loading mechanism, the relationship is given by Eq. (1). The schematic figure that represents the direction of load-carrying capacity is shown in Fig. 4.

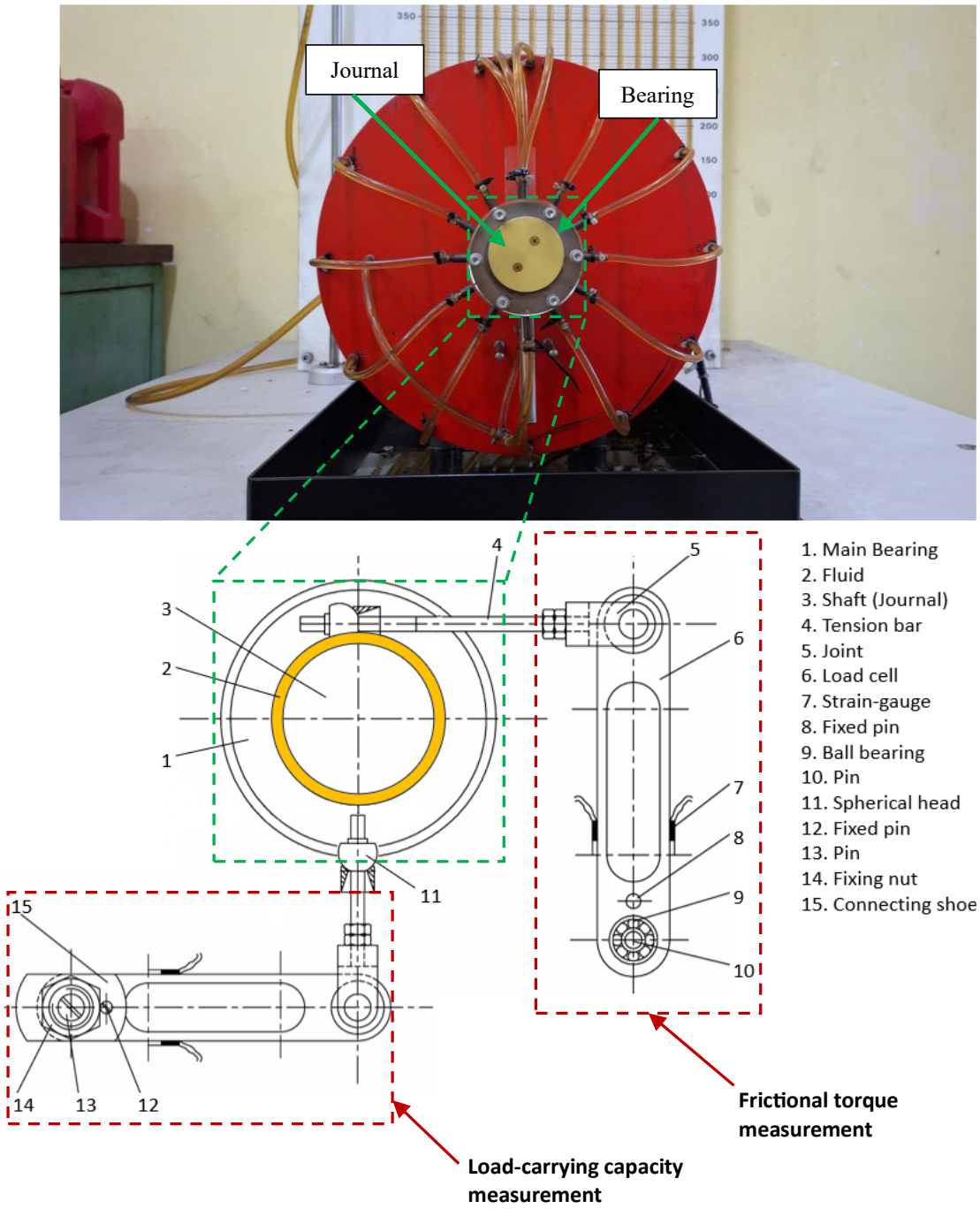

Fig. 3. Conceptual design of load-carrying capacity and frictional torque measurement.

$$W = \iint_A p \, dA = F_v \tag{1}$$

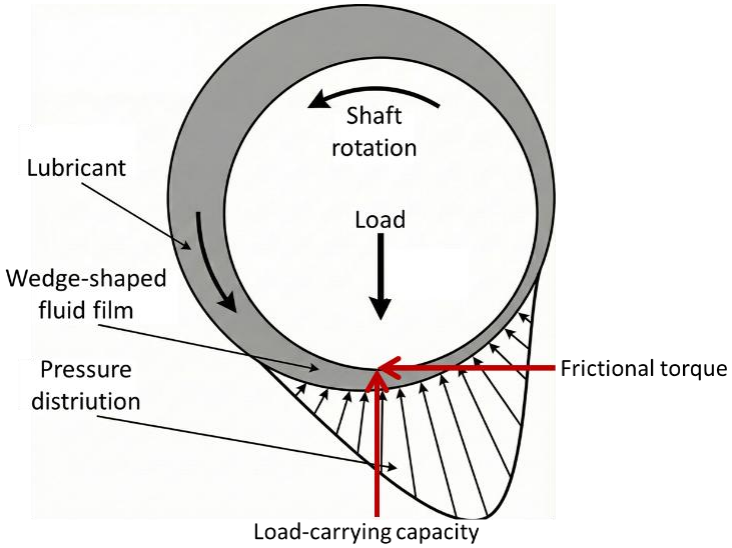

Fig. 4. Schematic diagram of load-carrying capacity and frictional torque.

Meanwhile, the frictional torque on the bearing is taken by the moment arm connected to the fixed pin (8) and the pin/bearing (9–10) that form the fixed support; the horizontal force (F_h) at the end of the arm is captured by the second load cell (6), so that the frictional torque (T) is calculated from the Eq. (2), where F_h is the force derived from the load cell and L is the effective length of the moment arm.

$$T = F_h \; L \tag{2}$$

To obtain the measurement data, a data acquisition system is required, as conceptually designed in Fig. 5. The architecture of the data acquisition system consists of a PC (1) acting as a user interface and data logger, Arduino Uno (2) as the acquisition controller, an OLED mini-LCD (3) as a real-time display. For force and torque measurements, the system employs two straight-bar aluminum load cells (4) (type YZC-131 or equivalent) with a capacity of 1 kg. These load cells have a rated output sensitivity of 1.0 ± 0.15 mV/V. They are interfaced with two HX711 modules (5), which function as signal amplifiers and 24-bit Analog-to-Digital Converters (ADC). The DS18B20 temperature sensor (7) to monitor lubricant temperature. To ensure the stability of the electrical signals, the load cells are powered with an excitation

voltage of 5V DC supplied directly through the HX711 modules. The data sampling rate for the HX711 was set to its standard 10 Hz (10 samples per second), which subsequently dictates the overall system update rate.

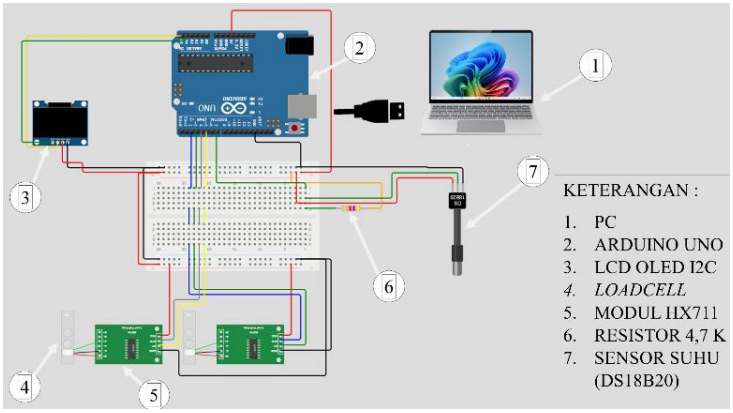

Fig. 5. Data acquisition system design.

The data acquisition process begins with a strain gauge-based load cell, which generates an analog potential difference signal, which is then amplified and digitized by the HX711 module. The output from the HX711 module is accessed by the Arduino via a separate DT/SCK pin pair, allowing the two channels to be acquired sequentially but synchronized. Each sample is time-stamped and combined with a temperature reading from the DS18B20, then packaged as a data packet. This data is forwarded to a computer via PLX DAQ software for display in Excel. Meanwhile, the main parameter values (force, torque, rpm, temperature) are displayed on an OLED mini-LCD for direct monitoring during the test.

2.3 Embodiment design

The developed system is based on the TM25 journal bearing demonstration. The rotating shaft (journal) is located within a lubricated bearing, forming a hydrodynamic lubrication film. Two measurement subsystems are designed according to design specifications.

The load force is measured by measuring the reaction force from the bearing housing, transmitted through a pull rod/bolt head mechanism to a load cell mounted on a rigid mount (as shown in Fig. 6). The load cell converts the force into an analog signal that is read by an Arduino/DAQ for real-time monitoring. The reaction torque is captured using a torque arm connected to the bearing housing. The force at the end of the arm is detected by a second load cell. The torque magnitude is calculated using Eq. (2). Both subsystems are mounted on a rigid frame to minimize misalignment, seal friction, and vibration.

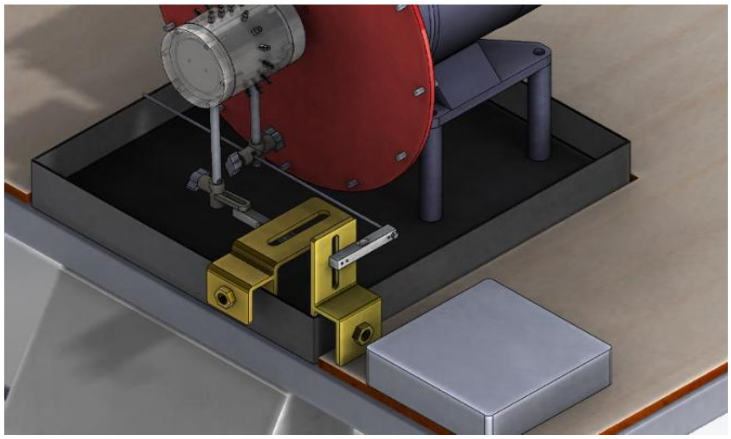

Fig. 6. 3D Design of journal bearing demonstration TM25 integrated load cell based measuring instrument.

3D modeling was performed using Solid works. The initial stage began with establishing the design intent and units in mm–N–s, followed by creating a parametric model using Global Variables and Equations. Datums (planes/axes) for the axle and reference planes were set up early to ensure the sketch was fully defined. The main components were then modeled as separate parts—adapter housing, torque arm, load cell bracket, baseplate, spacer/rod-end, and splash guard—using core features (Extrude, Cut, Hole Wizard, Fillet). Weldments were used for the frame, standard hardware was taken from the toolbox, and the material (steel and aluminum) was specified to ensure realistic mass and stiffness.

Assembly was performed in mating that maintained coaxiality and orthogonality; critical holes/mounts were created in-context and locked. Before release, Interference Detection and Clearance Verification were run, as well as quick validation with ANSYS Simulation. The quantitative results from the static analysis of the aluminum bar load cell showed a maximum deflection of only 0.017 mm and a minimum safety factor of 15 under an applied load of 10 N, confirming structural rigidity. This structural rigidity guarantees that the mechanical alignment of the load cells remains stable, preventing bias measurements. Load configuration and displacement results are visualized in Fig. 7. Furthermore, the modal analysis revealed that the fundamental (first) natural frequency of the assembly is 1782.4 Hz. This value is significantly higher than the maximum operating frequency of the rig, which is 50 Hz (at 3000 rpm), thereby safely avoiding any resonance issues. The corresponding mode shape from this modal analysis is visualized in Fig. 8. Finally, a complete A3/A4 drawing, BOM and exploded view along with tightening torques are prepared, then exported to STEP/Parasolid (manufacturing) and DXF/DWG. Design variations are managed concisely via Configurations/Design Table. The 3D modeling results can be seen in Fig. 6.

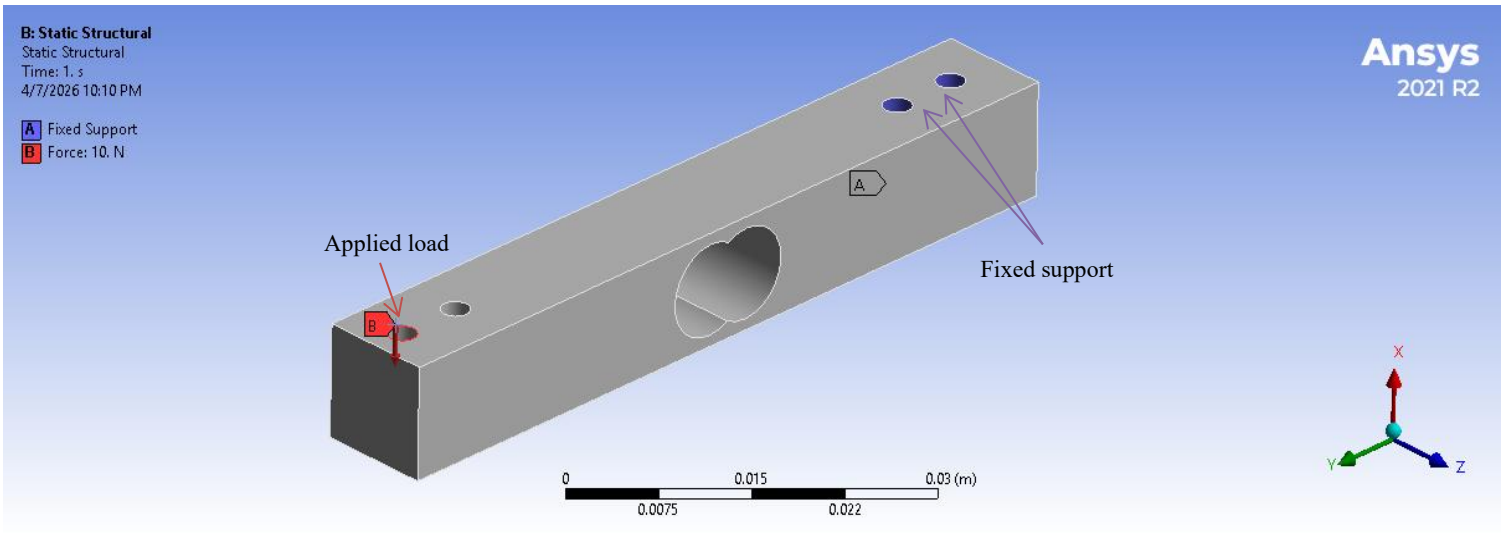

(a)

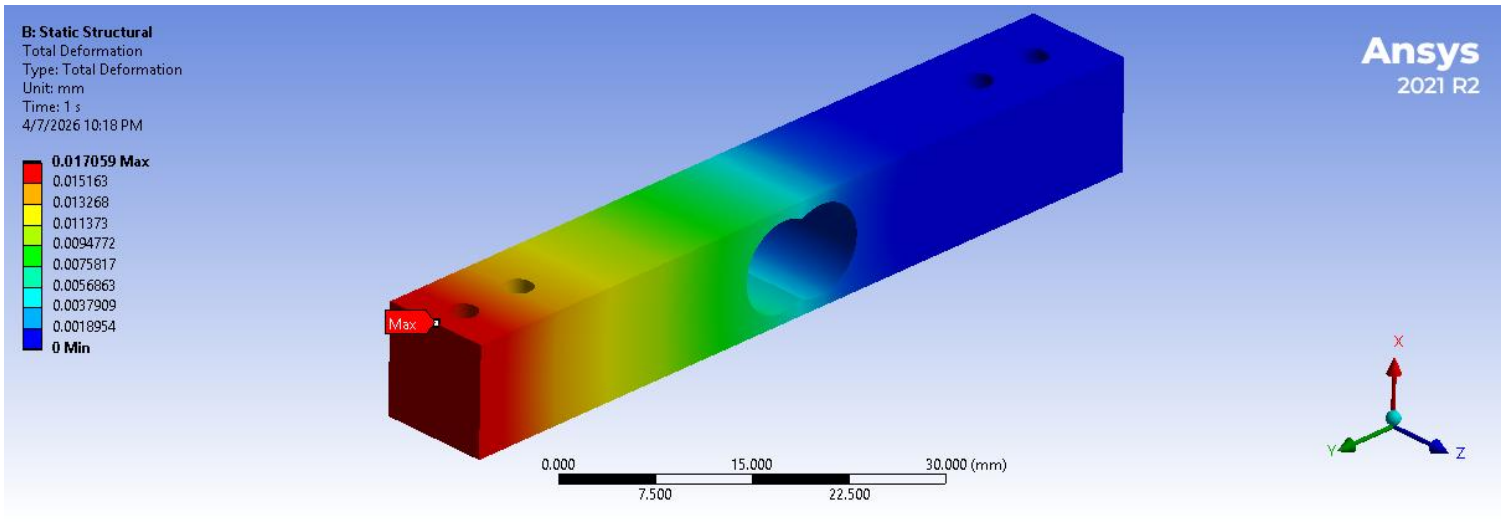

(b)

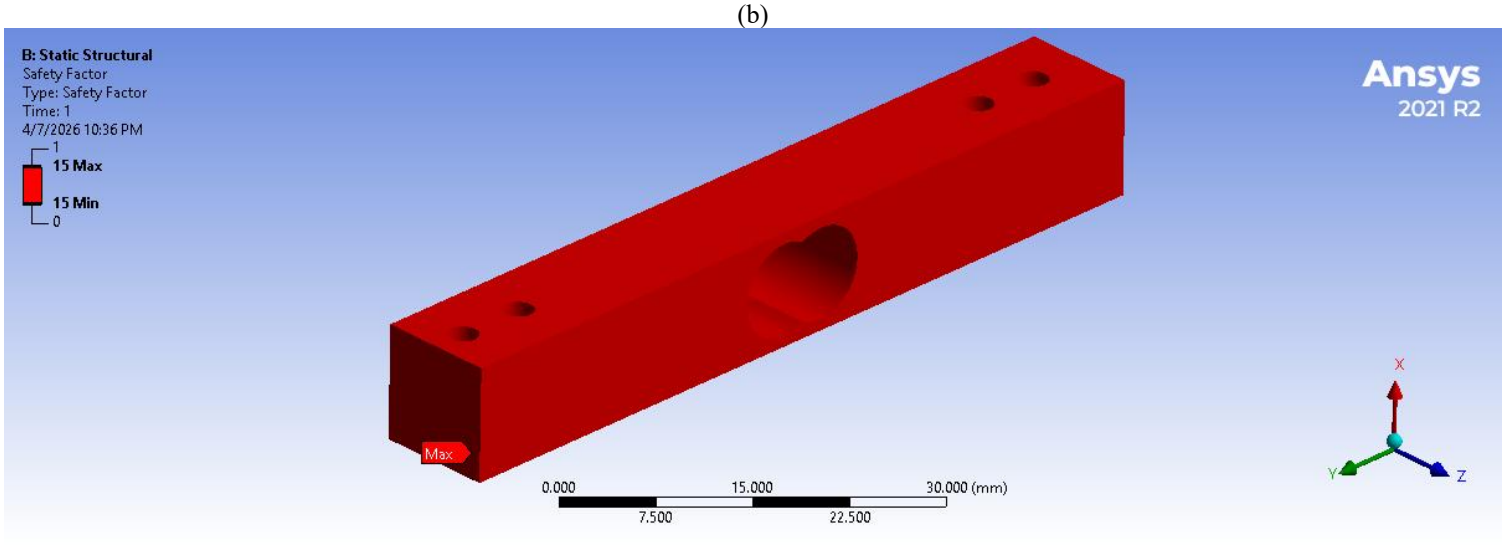

(c)

Fig. 7. Static structural analysis, (a) boundary conditions and applied load, (b) displacement results, (c) safety factor results.

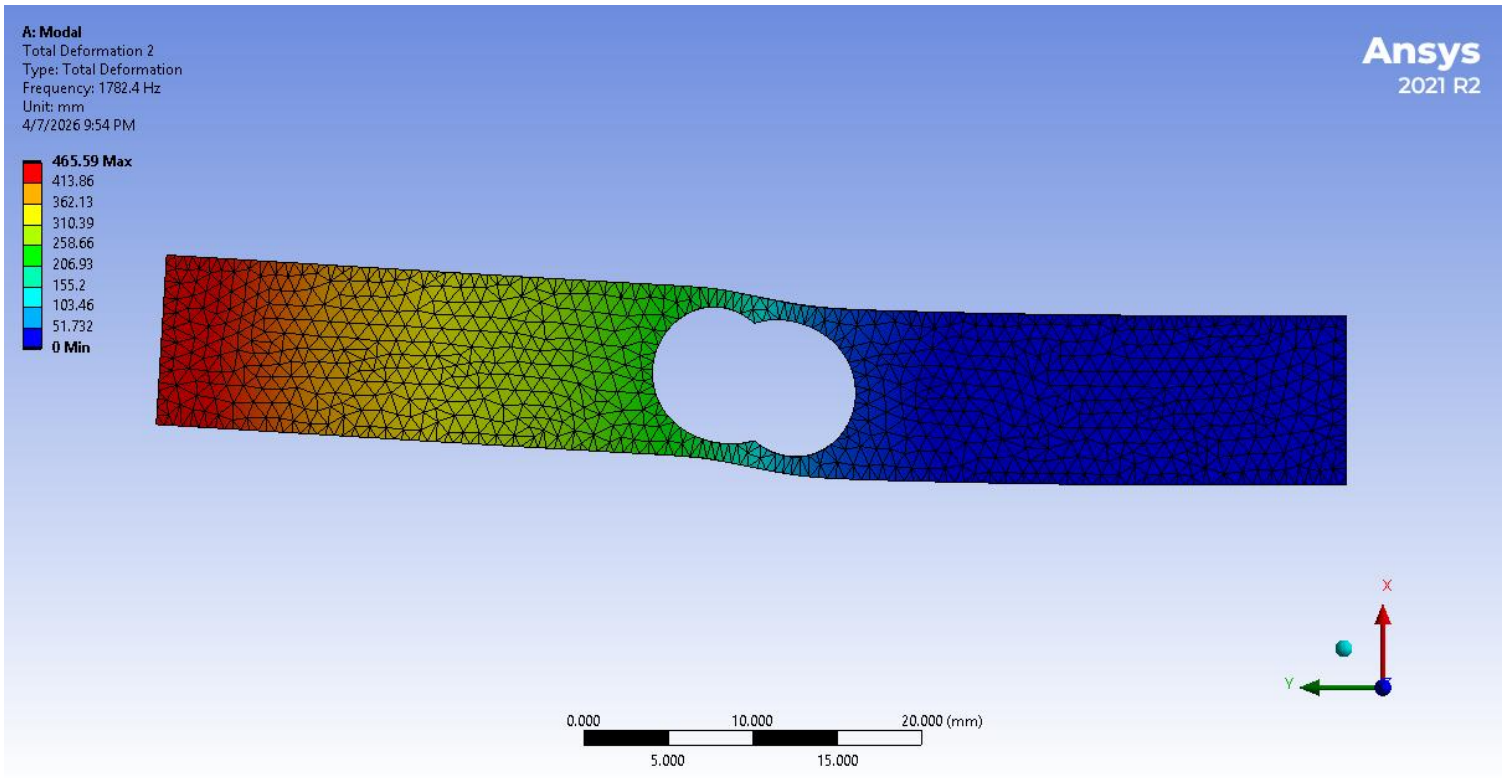

Fig. 8. The first mode shape at a natural frequency of 1782.4 Hz.

2.4 Load cell calibration

Before full assembly, both load cells pass a calibration process using traceable reference weights to establish a quantitative relationship between the actual and measured loads. The calibration utilized eight distinct load points ranging from 0 to 0.904 kg (specifically 0, 0.303, 0.403, 0.500, 0.607, 0.706, 0.803, and 0.904 kg). To ensure statistical reliability and reduce the effect of random noise or momentary fluctuations, three measurement repetitions

were recorded at each load point after a brief settling time. The averaged values were then analyzed using linear regression to determine the specific calibration factors for the Arduino data acquisition system. These factors enabled the accurate conversion of raw digital signals into precise physical units of force (N) and torque (Nm). Based on these repetitions, the expanded measurement uncertainty was evaluated to reach a confidence level.

For load cell 1, which functions as the load-carrying capacity gauge, the calibration data are detailed in Table 3 and presented in Fig. 9. The linear regression analysis yielded a highly proportional relationship, producing the mathematical model expressed in Eq. (3). The resulting coefficient of determination R^2 is 0.999996, indicating an exceptionally strong linear correlation. This near-perfect linearity confirms the sensor's high precision and measurement accuracy across the tested range.

$$y = -8.13 \times 10^{-5} + 0.9998\,x \quad (3)$$

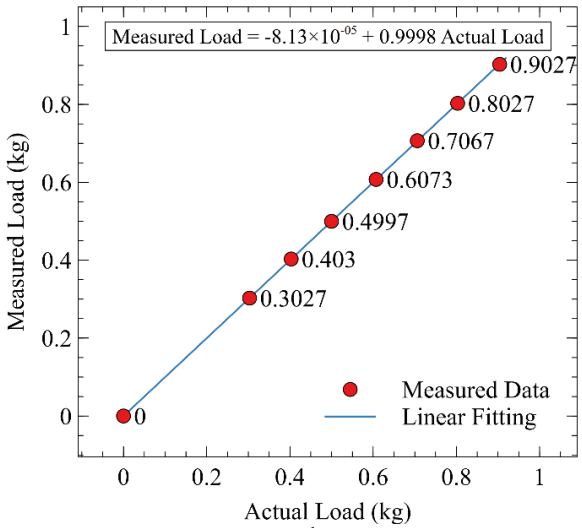

Fig. 9. Linear graph of the 3rd calibration of load cell 1.

Table 3. Calibration and conversion results of load cell 1

Actual load (kg)	1st measurement (kg)	2nd measurement (kg)	3rd measurement (kg)	Average (kg)
0	0	0	0	0.0000
0.303	0.302	0.303	0.303	0.3027
0.403	0.403	0.403	0.403	0.4030
0.5	0.499	0.5	0.5	0.4997
0.607	0.607	0.607	0.608	0.6073
0.706	0.706	0.707	0.707	0.7067
0.803	0.803	0.802	0.803	0.8027
0.904	0.902	0.903	0.903	0.9027

Similarly, for load cell 2, designated for frictional torque measurement, pass the identical calibration procedure. The corresponding results are detailed in Table 4 and presented in Fig. 10. The linear regression for this sensor produced the relationship shown in Eq. (4), with an R^2 value of 0.999997. This further verifies the reliability and exactness of the dynamic torque readings acquired by the modified testing platform.

$$y = 2.68 \times 10^{-4} + 0.9895\,x \quad (4)$$

Table 4. Calibration and conversion results of load cell 2

Actual load (kg)	1st measurement (kg)	2nd measurement (kg)	3rd measurement (kg)	Average (kg)
0	0	0	0	0.0000
0.303	0.3	0.3	0.3	0.3000
0.403	0.399	0.399	0.399	0.3990
0.5	0.495	0.495	0.495	0.4950
0.607	0.602	0.602	0.602	0.6020
0.706	0.699	0.699	0.699	0.6990
0.803	0.795	0.795	0.795	0.7950
0.904	0.894	0.894	0.894	0.8940

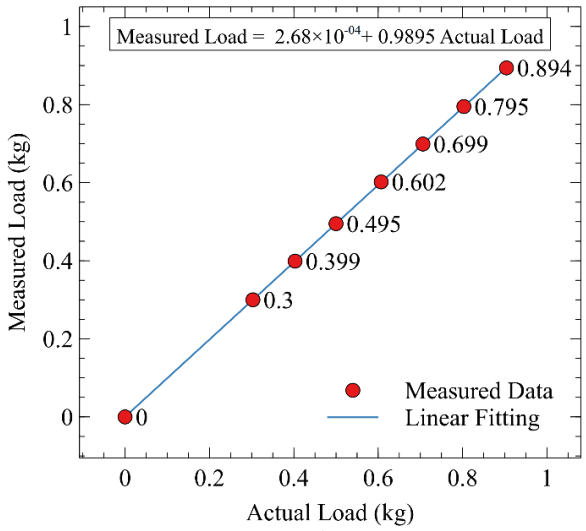

Fig. 10. Linear graph of the 2nd calibration of load cell 2.

2.5 Fabrication and assembly

The development of the TM25 journal bearing demonstration tester required the tools and materials. The tools and materials used included the TM25 journal bearing demonstration, connecting rod, Arduino, load cell, DS18B20 temperature sensor, HX711 amplifier, mini OLED LCD, jumper cables, 18650 Li-ion battery, lubricating oil, and supporting software such as Arduino IDE, Solidworks, and Microsoft Excel.

The development of the TM25 journal bearing tester was successful, with the addition of a load cell-based data acquisition system and a microcontroller. Modifications were made to several mechanical and electronic components to enable real-time measurement of load-carrying capacity and frictional torque. The results of the development as shown in Fig. 11.

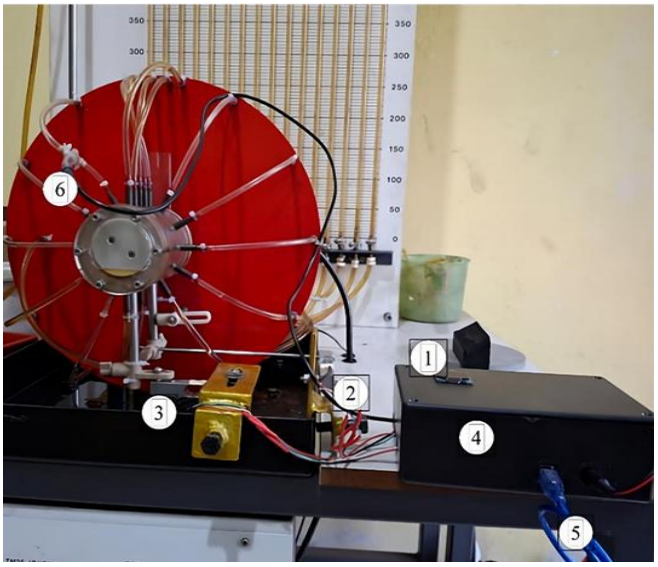

1. Mini LCD
2. Frictional torque load cell
3. Load-carrying capacity load cell
4. Microcontroller box
5. USB cable
6. DS18B20 temperature sensor

Fig. 11. Results of the development of the journal bearing demonstration TM25.

The mechanical components added include the creation of a load cell holder and a connecting socket between the balance pendulum and the sensor. The load cell holder is made of steel plate with a certain thickness to have adequate rigidity and minimize deformation when receiving force. The connecting socket is made with precision so that the load position is evenly distributed across the load cell surface. This modification aims to allow the reaction force from the journal bearing to be directly transmitted to the sensor, resulting in more accurate force readings. Several components such as the Arduino, battery, PCB board and mini LCD are placed inside the microcontroller box, as seen in Fig. 12.

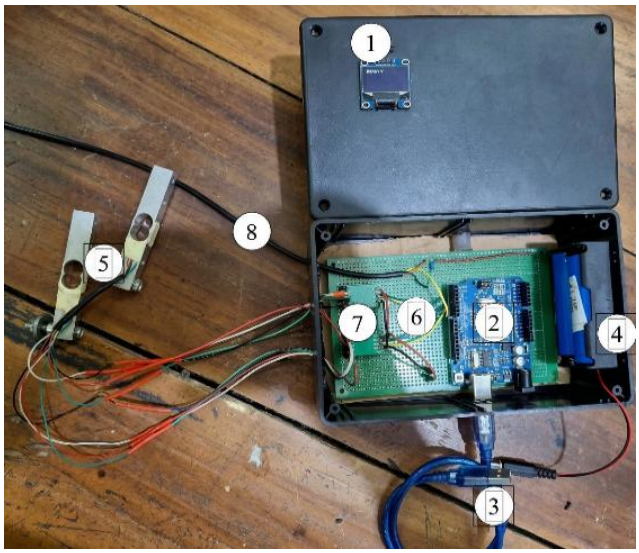

1. Mini LCD
2. Arduino
3. USB cable
4. Battery
5. Load cells
6. PCB
7. HX711 module
8. DS18B20 temperature sensor

Fig. 12. Microcontroller box.

3 Results and discussion

3.1 Pressure distribution on exsisting TM25 journal bearing demonstration

Hydrodynamic pressure distribution data was obtained through a manometer on the existing TM25 journal bearing demonstration. There are 16 manometer locations that measure hydrodynamic pressure along the circumferential and the axial direction of the journal bearing, as shown in Fig. 13. The circumferential direction pressure distribution shows the pressure variation data around the bearing, while the axial direction pressure distribution shows the pressure variation data along the axial axis of the bearing.

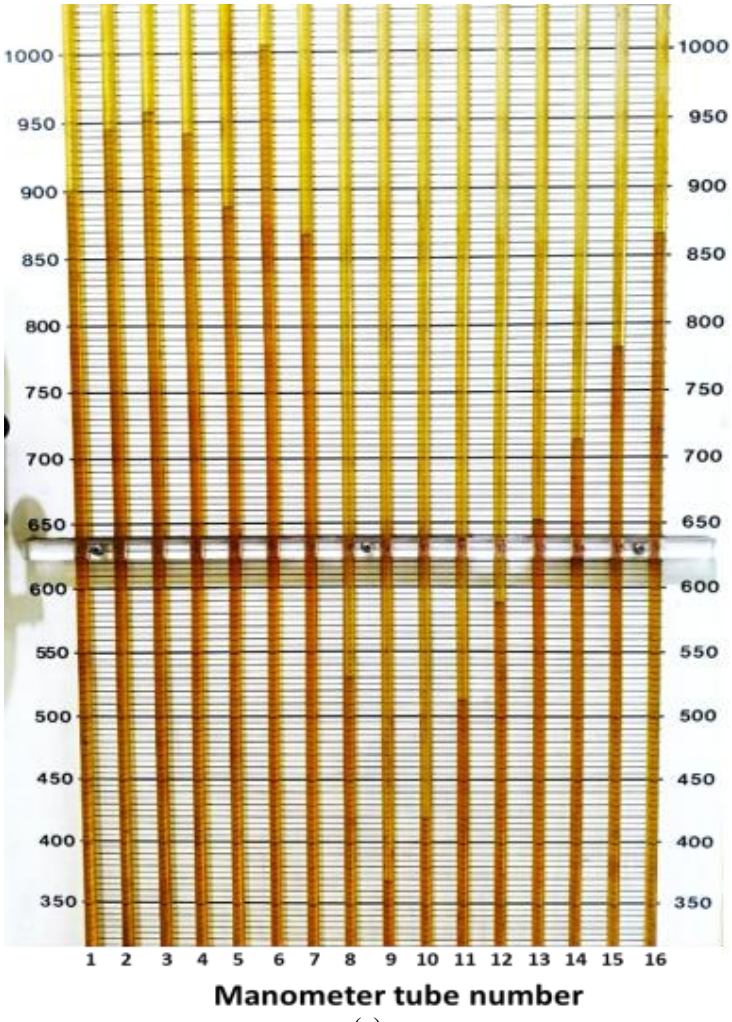

(a)

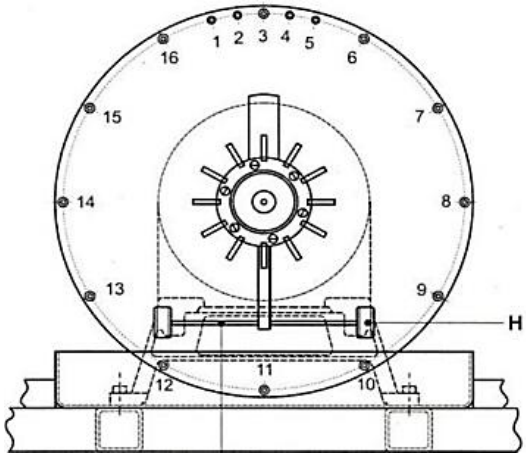

(b)

Fig. 13. Manometer location on existing TM25 journal bearing demonstration, (a) manometer tube, (b) circumferential direction.

Fig. 14 shows the axial pressure distribution of SAE 10W-30 lubricants for rotational speeds of 1000 rpm, 1250 rpm, 1500 rpm, 1750 rpm, and 2000 rpm. These data were collected using five manometers numbered 1 to 5 positioned along the bearing axial axis. For each rotational speed variation, the lubricant pressure curve is low at both ends of the bearing. The pressure peaks are at positions numbered 2 to 4 manometers, which represent the center of the bearing. This phenomenon is theoretically caused by the side leakage effect of lubricant from the bearing gap. As a result of this leakage, the lubricant pressure at the ends of the bearings drops to near atmospheric pressure. The observed pressure distribution appears relatively symmetrical about the center of the bearing axial axis. This indicates a harmonic operating condition of the bearing and a uniform side leakage effect on both sides.

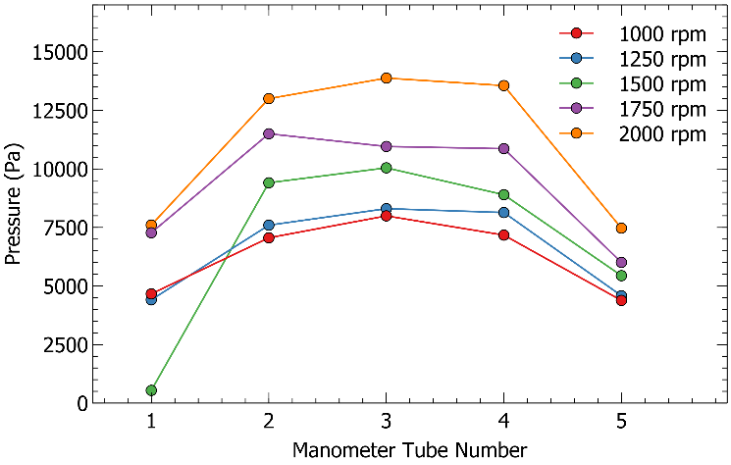

Fig. 14. Axial pressure distribution of SAE 10W 30 grade lubricant with variation of rotational speed.

Fig. 14 shows a clear positive trend between shaft rotational speed and lubricant pressure along the axial axis. As the rotational speed increases from 1000 rpm to 2000 rpm, the entire axial pressure distribution curve shifts significantly upward. This indicates that an increase in rotational speed corresponds to an increase in the overall lubricant pressure in the bearing clearance. This phenomenon of increased pressure due to increased rotational speed is consistent with the basic principles of hydrodynamic lubrication and can be explained by the Reynolds equation [20].

Furthermore, Fig. 15 illustrates the circumferential pressure distribution of the SAE 10W-30 lubricant for five rotation speeds, 1000-2000 rpm. These data were collected from manometers positioned around the circumference of the bearing. Unlike the relatively symmetrical axial distribution, the circumferential pressure profile exhibits a distinctly asymmetrical shape. The pressure gradually builds up from near-zero values at the fluid entry point, reaching a maximum peak around manometers 14 to 15

(270° to 300°). Following this peak, the pressure drops rapidly as it approaches manometers 11 to 12 (180° to 210°), returning to near-atmospheric levels. This asymmetrical pressure profile is a classic representation of the wedge effect [13]. This wedge effect is what generates the high hydrodynamic pressure required to support the applied load. The location of the peak pressure corresponds to the region immediately preceding the minimum film thickness.

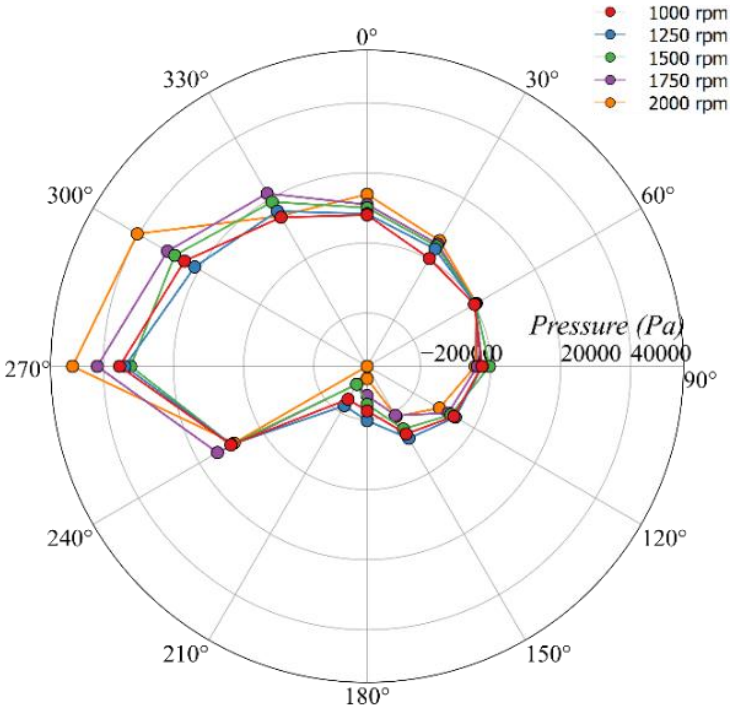

Fig. 15. Circumferential pressure distribution of SAE 10W 30 grade lubricant with variation of rotation speed.

Consistent with the axial data, Fig. 15 highlights a strong positive correlation between the rotational speed and the generated circumferential pressure. As the speed increases from 1000 rpm to 2000 rpm, the peak pressure magnitude increases substantially. For instance, at 1000 rpm, the maximum pressure is 35386 Pa, whereas at 2000 rpm, it more than doubles, reaching approximately 55165 Pa. This significant increase validates that higher rotational speeds produce load-carrying capacity, which aligns with the Reynolds equation [20].

3.2 Load cells measurement

The results of the load cell sensor readings are presented in Table 5, which shows the measurements obtained from the modified journal bearing demonstration test device.

Table 5. Measurement data on load cell 1 and load cell 2

Oil grade	Rotation speed (rpm)	Load cell 1 (kg)	Load cell 2 (kg)	Temperature (°C)
SAE 10W-30	1000	0.0313	0.0230	29.19
	1250	0.0335	0.0263	29.91
	1500	0.0391	0.0322	30.33
	1750	0.0394	0.0357	31.42
	2000	0.0396	0.0383	31.51
SAE 10W-40	1000	0.0432	0.0314	29.34
	1250	0.0492	0.0373	29.57
	1500	0.0581	0.0442	29.68
	1750	0.0631	0.0501	30.78
	2000	0.0714	0.0569	31.01
SAE 20W-50	1000	0.0644	0.0561	30.04
	1250	0.0824	0.0714	30.35
	1500	0.0929	0.0791	30.82
	1750	0.1048	0.0944	31.09
	2000	0.1213	0.1088	31.35

The presented data represent the calculated averages from measurements taken over a 15-minute duration for each test. During this period, a total of 300 data points were recorded, corresponding to a precise data logging interval of 3 seconds per sample. In this test, load cell 1 is used to measure the vertical upward force (load-carrying capacity) that works due to the pressure of the lubricating fluid on the shaft surface. Meanwhile, load cell 2 functions to measure the tangential force (frictional force) that is directly related to the frictional torque that occurs during shaft rotation. The raw values from both sensors are initially read in kilograms (kg) and subsequently converted into force units of Newtons (N). The force data from load cell 2 is then used to calculate the frictional torque (Nm) using Eq. (2). The results of frictional torque measurements produced by real-time measurements using Arduino and load cell sensors can be seen in Table 6.

Table 6. Frictional torque from load cell measurement

Rotation speed (rpm)	Frictional torque (Nm)		
	Oil grade 10W 30	Oil grade 10W 40	Oil grade 20W 50
1000	0.0270	0.0369	0.0660
1250	0.0310	0.0439	0.0840
1500	0.0379	0.0519	0.0930
1750	0.0420	0.0589	0.1110
2000	0.0450	0.0669	0.1279

Based on Table 6, a graph of the effect of rotational speed on frictional torque for the three types of oil can be obtained. The graph can be seen in Fig. 16. The frictional torque graph shows an increasing trend in the value of frictional torque as the rotational speed (rpm) increases for all types of oil. The resulting frictional torque value is directly proportional to the viscosity of the lubricant. 20W-50 oil produces the highest frictional torque, followed by 10W-40, while 10W-30 produces the lowest value. This phenomenon is in accordance with the theory of hydrodynamic lubrication (Petroff's equation) shown in Eq. (4), where friction in full lubrication conditions (hydrodynamic lubrication) is caused by the shear stress of the fluid (shear stress) on the lubricant film [21], [22].

$$f = 2\pi^2 \frac{\mu N}{P} \frac{r}{c} \tag{4}$$

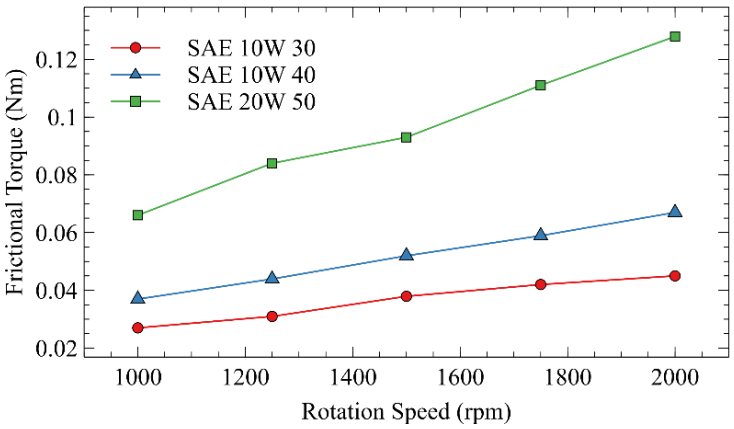

Fig. 16. The effect of rpm on frictional torque.

The magnitude of the shear stress is determined by two primary factors: the rotational speed (N) and the fluid viscosity (μ). A higher rotational speed induces a greater velocity gradient within the lubricant film, thereby increasing the shear force. Similarly, a higher viscosity results in greater fluid resistance to flow, which in turn elevates the generated frictional torque. Consequently, these experimental results are highly consistent with the theoretical principle that frictional torque is directly proportional to both the fluid viscosity and the rotational speed.

The results of the load-carrying capacity measurements produced by real-time measurements using Arduino and load cell

sensors are shown in Table 7. Based on Table 7, a graph of the load-carrying capacity is obtained for each variation of rotation speed and the type of oil. The graph of the load-carrying capacity obtained from the experimental results can be seen in Fig. 17.

Table 7. Load-carrying capacity from load cell measurement

Rotation speed (rpm)	Load-carrying capacity (N)		
	Oil grade 10W 30	Oil grade 10W 40	Oil grade 20W 50
1000	0.307	0.423	0.631
1250	0.328	0.482	0.808
1500	0.383	0.569	0.910
1750	0.386	0.618	1.027
2000	0.388	0.700	1.189

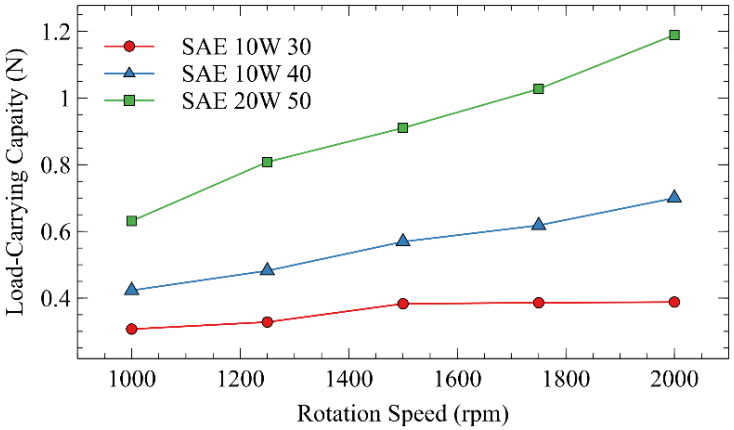

Fig. 17. The effect of rpm on load-carrying capacity.

Fig. 17 shows an increase in load-carrying capacity as shaft rotational speed increases. At low rotational speeds (1000 rpm), the load-carrying capacity is relatively small, but increases significantly at higher rpms (2000 rpm). This is due to the greater hydrodynamic pressure generated by the increased wedge effect in the lubrication gap. 20W-50 oil exhibits the highest load-carrying capacity, reaching 1.189 N at 2000 rpm.

This is because the higher viscosity allows for the formation of a thicker lubricant film and greater hydrodynamic pressure. In contrast, 10W-30 oil can only produce a load-carrying capacity of approximately 1.09 N at 2000 rpm, which is relatively small due to its thinner lubricant film. 10W-40 oil is in between the two with a maximum load-carrying capacity of 1.46 N. This result is in line with Reynolds' theory which states that the bearing load-carrying capacity increases with increasing viscosity and rotational speed [2], [23], [24].

To further validate the accuracy of the modified measurement system, it is crucial to establish the physical relationship between the localized hydrodynamic pressure distribution observed via the existing manometers, as shown in Fig. 14 and Fig. 15 and the global load-carrying capacity recorded by the integrated load cells, as shown in Fig. 17. According to fundamental hydrodynamic principles, the total load-carrying capacity of a journal bearing is mathematically derived from the integral of the fluid film pressure over the effective bearing surface area [25].

As previously established, an increase in rotational speed, from 1000 rpm to 2000 rpm, significantly elevates the entire axial and circumferential pressure distribution from manometer measurement. Consequently, this accumulation of higher pressure distribution directly translates into a higher load-carrying capacity for the journal bearing. This correlation between an existing journal bearing demonstration and the modified journal bearing demonstration serves as a validation, proving the reliability of the developed acquisition system.

3.3 Comparisson to lubrication theory

To validate the experimental measurements, the actual frictional torque acquired from the load cell was compared against the theory of frictional torque using Petroff's equation which is derived from the Eq. (4). The frictional torque equation is shown in Eq. (5). The comparative data for different lubricant grades across varying rotation speeds are presented in Fig.18.

$$T = \frac{4\pi^2 r^3 \mu N L}{c} \tag{5}$$

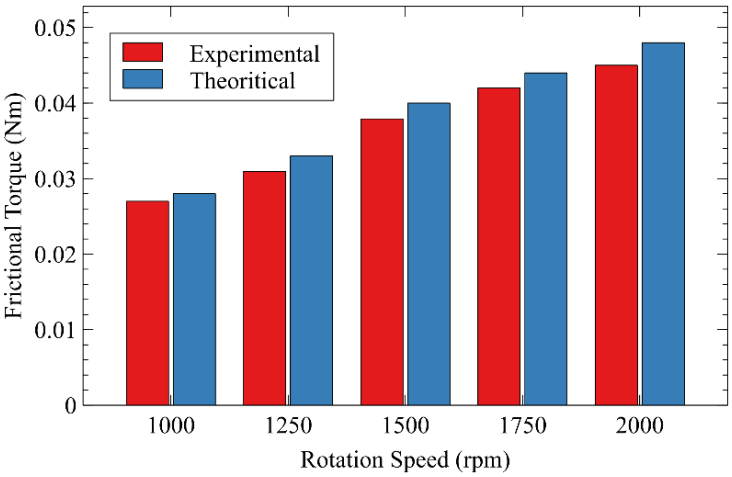

Fig. 18. Comparison of frictional torque between experimental results (load cell) and theoretical calculations (Petroff equation) of SAE 10W 30.

As observed, both the experimental and theoretical frictional torques exhibit a proportional linear increase in shaft rotational speed and lubricant viscosity. However, a consistent deviation exists, where the experimental torque is slightly lower than the theoretical across all measured points. For instance, evaluating the system at the specific operating point of 2000 rpm using SAE 10W-30 oil, the expected theoretical frictional torque calculated via Petroff's equation is 0.048 Nm. In contrast, the actual measured torque recorded by the sensor is 0.045 Nm. This results in a relatively small deviation of approximately 6%, as shown in Fig. 18.

This numerical difference can be explained by examining the ideal assumptions in Petroff's equation. Petroff's equation assumes a perfectly concentric shaft (zero eccentricity) in journal bearing, zero side leakage, and a constant fluid viscosity throughout the operation. In the actual experimental setup, the shaft operates with a certain degree of eccentricity due to the hydrodynamic pressure distribution. More importantly, the continuous fluid shearing at high rotational speeds generates localized heat within the lubricant film. This localized temperature rise causes a slight reduction in the effective dynamic viscosity of the oil inside the clearance compared to its assumed temperature state in Petroff's equation. Consequently, the actual viscous shear resistance and thus the measured frictional torque are slightly lower than the theoretical. Despite these minor deviations, the experimental trends perfectly reflect the theoretical principles, validating the accuracy and reliability of the modified real-time data acquisition system.

4 Conclusions

This research successfully modified the TM25 journal bearing demonstration unit into a journal bearing test rig equipped with load cell-based measurements for real-time load-carrying capacity and frictional torque. The data acquisition system was connected to a PC via Excel Data Streamer, with numerical output displayed on a mini-OLED LCD. Calibration results showed a deviation of less than 2%, indicating stable and reliable sensor performance within the tested load range. This modification extends the capability of the TM25 unit beyond pressure distribution measurement to include dynamic load and frictional torque evaluation. The experimental results showed a clear increase in both load-carrying capacity and frictional torque with increasing shaft rotational speed

and lubricant viscosity. Higher viscosity oil (SAE 20W-50) produced the highest load-carrying capacity and frictional torque, while SAE 10W-30 yielded the lowest values. These results are consistent with hydrodynamic lubrication theory, where increased viscosity and rotational speed improve oil film pressure and resistance. This study has several limitations, the current sensor configuration measures load only in the vertical direction, whereas actual journal bearing forces include both vertical and horizontal components. In addition, load-carrying capacity and frictional torque cannot be measured simultaneously due to mechanical constraints. Future work should focus on multi-axis force measurement, simultaneous torque-load acquisition, and improved temperature sensing directly within the bearing housing.

Acknowledgment

The authors would like to express their gratitude to the University of Lampung through the Institute for Research and Community Service (LPPM) for the support and trust provided through the DIPA BLU 2025 Research Grant under contract No.2107/UN26.15/LK.03/2024, which has greatly contributed to the implementation of this study.

References

[1] S. Chaudhary and R. Verma, "A Comprehensive Review of Journal Bearing Models: Comparative Analysis of Thermal, Elastic, and Hydrodynamic Approaches Considering Misalignment, Surface Texture, Turbulence, and Cavitation," *J. Tribol*, vol. 147, no. 110802, Aug. 2025, doi: 10.1115/1.4069141.

[2] B. J. Hamrock, S. R. Schmid, and B. O. Jacobson, *Fundamentals of fluid film lubrication*, 2nd ed. in Mechanical engineering, no. 169. New York: Marcel Dekker, 2004.

[3] M. M. Khonsari and E. R. Booser, *Applied tribology: bearing design and lubrication*, Third Edition. in Tribology Series. Hoboken, New Jersey: Wiley, 2017.

[4] TecQuipment, "JOURNAL BEARING DEMONSTRATION," TecQuipment. Accessed: Oct. 14, 2025. [Online]. Available: https://www.tecquipment.com/journal-bearing-demonstration

[5] J. Fraden, *Handbook of modern sensors: physics, designs, and applications*, Fifth edition. in SpringerLink Bücher. Cham Heidelberg New York Dordrecht London: Springer, 2016. doi: 10.1007/978-3-319-19303-8.

[6] N. Marey, E.-S. Hegazy, and A. Aly, "Design and Setup for a Journal Bearing Universal Test Rig," *Port-Said Engineering Research Journal*, vol. 22, pp. 101–106, Mar. 2018, doi: 10.21608/pserj.2018.32472.

[7] A. Biyiklioglu, H. Cuvalci, H. Adatepe, H. Bas, and M. S. Duman, "A NEW TEST APPARATUS AND METHOD FOR FRICTION FORCE MEASUREMENT IN JOURNAL BEARINGS UNDER DYNAMIC LOADING: Part I," *Experimental Techniques*, vol. 29, no. 5, pp. 22–24, Sep. 2005, doi: 10.1111/j.1747-1567.2005.tb00235.x.

[8] A. Biyiklioglu, H. Cuvald, H. Adatepe, H. Bas, and M. S. Duman, "A NEW TEST APPARATUS AND METHOD FOR FRICTION FORCE MEASUREMENT IN JOURNAL BEARINGS UNDER DYNAMIC LOADING: PART II," *Experimental Techniques*, vol. 29, no. 6, pp. 33–36, Nov. 2005, doi: 10.1111/j.1747-1567.2005.tb00244.x.

[9] A. G. Chavan and Y. P. Reddy, "Numerical Investigation of Short Bearing Lubricated with Copper Oxide Nanolubricants," *Tribol. Ind.*, vol. 46, no. 2, pp. 198–209, Jun. 2024, doi: 10.24874/ti.1476.04.23.10.

[10] S. Beamish and R. S. Dwyer-Joyce, "Experimental Measurements of Oil Films in a Dynamically Loaded Journal Bearing," *Tribology Transactions*, vol. 65, no. 6, pp. 1022–1040, Oct. 2022, doi: 10.1080/10402004.2022.2106926.

[11] P. Wang *et al.*, "Numerical Analysis on the Static Performance of Gas Journal Bearing by Using Finite Element Method," *Nanomanuf Metrol*, vol. 7, no. 1, pp. 1–20, Dec. 2024, doi: 10.1007/s41871-023-00219-0.

[12] F. V. Silva, M. A. Zanardi, and T. M. De Souza, "Analytical–numerical modeling of journal bearings with non-Newtonian fluids and cavitation effects," *J Braz. Soc. Mech. Sci. Eng.*, vol. 43, no. 12, p. 525, Dec. 2021, doi: 10.1007/s40430-021-03238-4.

[13] M. Tauviqirrahman, M. Wijaya, M. Muchammad, P. Paryanto, and J. Jamari, "Hydrodynamic lubrication analysis of journal bearing considering cavitation, slip and thermal condition," *J. Tribol*, vol. 42, pp. 1–20, 2024.

[14] T. N. Babu, T. M. Raj, and T. Lakshmanan, "A Review on Application of Dynamic Parameters of Journal Bearing for Vibration and Condition Monitoring," *Journal of Mechanics*, vol. 31, no. 4, pp. 391–416, Aug. 2015, doi: 10.1017/jmech.2015.6.

[15] A. Ali and R. Zarhan, "Kaji Teoritik Distribusi Tekanan pada Journal Bearing," *Jurnal Rekayasa Energi dan Mekanika*, vol. 3, no. 2, Art. no. 2, 2023, doi: 10.26760/JREM.v3i2.95.

[16] H. Yi, H. Jung, K. Kim, and K. Ryu, "Static Load Characteristics of Hydrostatic Journal Bearings: Measurements and Predictions," *Sensors*, vol. 22, no. 19, 2022, doi: 10.3390/s22197466.

[17] D. Karki, H. B. Dura, and L. Poudel, "Design, construction and performance analysis of dynamic torque transducer," *Journal of Innovations in Engineering Education*, vol. 6, no. 1, pp. 118–123, Dec. 2023, doi: 10.3126/jiee.v6i1.43809.

[18] H. B. Harja, R. A. Febriani, N. Saksono, M. Y. Diratama, and M. Fauzi, "Design and development of a radial air bearing concave profile for an educational tool," *Jurnal Polimesin*, vol. 23, no. 5, pp. 637–642, Oct. 2025, doi: 10.30811/jpl.v23i5.7216.

[19] TecQuipment, "TM25 Journal Bearing Demonstration User Guide." TecQuipment, 2014.

[20] Y. Hori, *Hydrodynamic lubrication*. Tokyo ; New York: Springer, 2006.

[21] J.-L. Ligier and B. Noel, "Friction Reduction and Reliability for Engines Bearings," *Lubricants*, vol. 3, no. 3, pp. 569–596, Sep. 2015, doi: 10.3390/lubricants3030569.

[22] N. Marey, "An experimental investigation of hydrodynamic journal bearing with different oil grades," *Port-Said Engineering Research Journal*, vol. 23, no. 2, pp. 46–54, 2019.

[23] P. Zulhanafi, S. Syahrullail, and M. A. Ahmad, "The Tribological Performance of Hydrodynamic Journal Bearing Using Bio-based Lubricant," *Tribol. Ind.*, vol. 42, no. 2, pp. 278–287, Jun. 2020, doi: 10.24874/ti.843.02.20.05.

[24] G. H. G. Van Der Meer, F. Quinci, W. Litwin, M. Wodtke, and R. A. J. Van Ostayen, "Experimental comparison of the transition speed of a hydrodynamic journal bearing lubricated with oil and magnetorheological fluid," *Tribology International*, vol. 189, p. 108976, Nov. 2023, doi: 10.1016/j.triboint.2023.108976.

[25] M. Muchammad, M. Tauviqirrahman, Y. M. Rizki, I. Syafaat, F. Maharani, and M. I. Ammarullah, "Elastohydrodynamic analysis of multistep texture effects and partial surface roughness on the tribological performance of steel journal bearings," *Discov Appl Sci*, vol. 7, no. 4, p. 301, Apr. 2025, doi: 10.1007/s42452-025-06789-6.